Cellulose (2021) 28:9069–9079
https://doi.org/10.1007/s10570-021-04124-x

ORIGINAL RESEARCH

# Detection and quantitation of cellulose II by Raman spectroscopy

**Umesh P. Agarwal · Sally A. Ralph · Carlos Baez · Richard S. Reiner**

Received: 26 May 2021 / Accepted: 29 July 2021 / Published online: 13 August 2021


**Abstract** In cellulose materials, the cellulose II allomorph is often present either exclusively or in conjunction with cellulose I, the natural cellulose. Moreover, in regenerated and mercerized fibers (e,g., lyocell and viscose), natural cellulose adopts to the crystal structure cellulose II. Therefore, its detection and quantitation are important for a complete assessment of such materials investigations. In the Raman spectra of such materials, a band at 577 $cm^{-1}$ is typically observed indicating the presence of this allomorph. In the present study, to quantify the content of cellulose II, a calibration method was developed based on the intensity of the 577 $cm^{-1}$ peak relative to the 1096 $cm^{-1}$ band of cellulose. For this purpose, in addition to pure cellulose I and cellulose II samples (respectively, Avicel PH-101 and mercerized Avicel PH-101; hence referred to as Avicel I and Avicel II), a set of five samples were produced by mixing them in known quantities of Avicel I and Avicel II. The crystalline cellulose II contents of the samples were calculated based on the X-ray crystallinity of mercerized Avicel I. These seven samples were included in the calibration set and their Raman spectra were obtained. Subsequently, Raman intensity ratios $I_{577}/I_{1096}$ were calculated by taking ratios of peak intensities at 577 and 1096 $cm^{-1}$. These ratios were plotted against the % of crystalline cellulose II present in the calibration set samples and the two were found to be linearly correlated ($R^2 = 0.9944$). The set-samples were also analyzed using XRD which were then compared with the Raman method developed here. Compared to XRD, the Raman method was found to be more sensitive at detecting and quantifying cellulose II. Additionally, several cellulose II containing materials were analyzed by the new Raman method.

**Supplementary Information** The online version contains supplementary material available at https://doi.org/10.1007/s10570-021-04124-x.

U. P. Agarwal (✉) · S. A. Ralph · C. Baez · R. S. Reiner
Fiber and Chemical Sciences Research, USDA FS, Forest Products Laboratory, 1 Gifford Pinchot Drive, Madison, WI 53726-2398, USA
e-mail: umesh.p.agarwal@usda.gov

## Graphic abstract

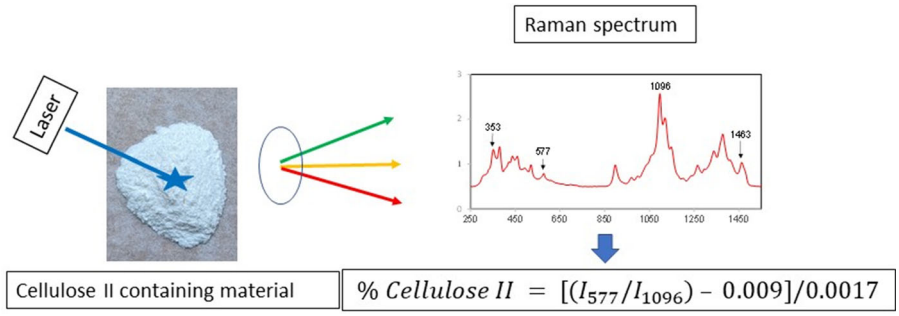


**Keywords** Regenerated cellulose · NaOH treated · Polymorphs · Raman spectroscopy · Quantitation · X-ray diffraction

## Introduction

Raman spectroscopy is being increasingly used to investigate celluloses and cellulose based materials (Agarwal 2019; Agarwal et al. 2021a; Agarwal et al. 2021b; Gierlinger 2018; Kanbayashi et al. 2021; Kesari et al. 2020; Morgan et al. 2019). Although many research areas have benefitted from such applications, one of the areas of high importance is characterization of cellulose supramolecular structure. Understanding of the structure is important to many areas of bioeconomy R & D, e.g., biofuels (Callegari et al. 2020) and nanocellulose based materials (Foster et al. 2018), where improved characterization is needed to better understand how different process conditions affect the structure of cellulose. Towards meeting that objective, Raman spectroscopy has made several advances. For instance, to estimate cellulose crystallinity, methods based on three different Raman peaks are available-namely 1481, 380, and 93 $cm^{-1}$ (respectively, Schenzel et al. 2005; Agarwal et al. 2010, 2018). Furthermore, additional methods were developed to characterize other structural features of cellulose. These consist of accessibility to water (Agarwal et al. 2016; Foster et al. 2018), degree of lateral order (DOLO) (Agarwal et al. 2016), exocyclic C6 $CH_2OH$ conformation (Agarwal et al. 2018, 2021b), and chain conformational disorder (CCONDIS) (Agarwal et al. 2021b). Considering that the other existing methods have limitations to fully characterize the supramolecular structure of cellulose, such contribution of Raman spectroscopy is a welcome development.

Cellulose can exist in various crystalline forms and therefore, is a polymorphic material. There are several distinct known crystalline forms-cellulose I, cellulose II, cellulose III, and cellulose IV, although the existence of cellulose IV is still debated (Wada et al. 2004, 2006). For instance, cellulose $IV_I$ and cellulose $IV_{II}$ are, respectively, considered disordered forms of cellulose I and cellulose II, or in the case of cellulose $IV_{II}$, as a mixture of cellulose I and cellulose II (Wada et al., 2004). Moreover, for cellulose I, two distinct crystalline forms have been proposed–Iα and Iβ (Atalla & VanderHart, 1984). Cellulose II (also referred to as regenerated or mercerized cellulose) is the other most often used allomorph. The regenerated form is produced by dissolution in various solvents and subsequent re-solidification—e.g., from ionic liquids (Sixta et al. 2015) and the mercerized form is produced by rinsing and drying NaOH-swollen cellulose (Porro et al. 2007). The NaOH swollen cellulose form is used in viscose/rayon manufacture in the textile and fiber industries (Kumar and Christopher 2017). Cellulose II is also formed during many laboratory and industrial processes; e.g., in cellulose nanocrystal production during the early stages of sulfuric acid hydrolysis of wood-pulps (Xing et al. 2018), in the manufacturing of dissolving pulps (Chen et al. 2016), and in the production of regenerated cellulose for use in textile fibers (Sixta et al. 2015). Mercerization to produce cellulose II is used in the textile industry to help natural fibers gain shine, dyeability, and strength. Moreover, the same process

is used as an activation step for many industrial products such as cellulose derivatives, regenerated fibers, and cellulose-based sponges. From a structural point of view, cellulose I and cellulose II allomorphs differ not only in that their H-bonds are different, but also conformations of the chains and the local exocyclic $C_6$ hydroxyl groups are different (Atalla 1976, 1983, 1989). Additionally, contrary to cellulose I where the chains have parallel orientation, in cellulose II, the chains are stacked with opposite polarity, also called an antiparallel structure (Langan et al. 2001).

Because the properties of the cellulose II allomorph are different from those of cellulose I (Sixta et al. 2015), the characterization of the former is essential. For that purpose, some of the often-used methods consist of X-ray, NMR and Raman spectroscopy (Nam et al. 2016; Nishiyama et al. 2000; Atalla et al. 1980; Haslinger et al. 2019; Atalla 1976; Schenzel and Fischer 2001). Amongst these techniques, XRD has been used the most to detect and obtain information on cellulose II (Zugenmaier 2010). However, in materials where both cellulose I and cellulose II allomorphs are simultaneously present, typically, in most methods, such analyses are based on the separation of cellulose II contributions from the contributions of cellulose I. Therefore, the analyses remain somewhat subjective, especially when there is significant overlap between the contributions.

Traditional Raman spectroscopy has been applied for a long time in the analysis of cellulose materials, but due to sample-fluorescence contributions to the spectra, it was not until FT-Raman spectroscopy became available that high signal-to-noise spectra could be obtained (Agarwal and Ralph 1997; Agarwal 1999; Schenzel and Fischer 2001). The first FT-Raman study of the transformation of cellulose I to cellulose II allomorph was reported in 2001 (Schenzel and Fischer 2001). Subsequently, in 2009, a multivariate calibration model based on FT Raman spectroscopy was developed to quantify cellulose I to cellulose II allomorphic transformation (Schenzel et al. 2009). However, this chemometric method is somewhat involved and not very user-friendly. Our intent was to develop a simple and more convenient Raman method. Previously, Agarwal (Agarwal 2014) had compared the FT-Raman spectra of the three cellulose allomorphs (cellulose I, cellulose II, and cellulose III) and noted spectral differences between them in the conformation sensitive region ($< 1500\ cm^{-1}$). Based on that information, cellulose I and cellulose II can be distinguished easily. In particular, the existence of a band at $577\ cm^{-1}$ in the spectrum of cellulose II can be seen which is not detected in the spectra of cellulose I and amorphous cellulose.

In many materials amorphous cellulose is also present along with the cellulose I and cellulose II. It is critical that spectral features that are unique to cellulose II which do not overlap with the other Raman peaks in the spectrum of amorphous cellulose be used in its quantitation. Therefore, in this study, detection and quantitation of cellulose II was carried out using this $577\ cm^{-1}$ band.

## Materials and methods

### Chemicals and materials

Avicel PH-101 (cellulose I) and Avicel-C (cellulose II) were obtained from American Viscose Division and Chemical Division of FMC Corporation, Newark, Delaware. Amorphous Avicel PH-101 cellulose was generated by grinding, for total time of 120 min, in a vibratory ball mill using steel balls (Forziati et al. 1950) and the milling was conducted in a cold room (5 °C). For this, in a 1 L jar, 300 1/4" diameter balls were used for milling. The grinding of 5 g cellulose was carried out by milling for 30 min, then no milling for the next 30 min and so on. Further details were exactly as in the reference cited. All other chemicals and reagents, unless stated otherwise, were purchased from Sigma-Aldrich (St. Louis, MO). Softwood bleached kraft pulp was from NewPage Corporation, Miamisburg, Ohio. Rayon-grade dissolving wood pulp used in the production of cellulose nanocrystals (CNCs) was obtained from Rayonier Mill in Jesup, GA.

### Cellulose II preparation

Cellulose II was produced by mercerization following the method of Hirota (Hirota et al. 2010) with slight modification. The method consisted of soaking the Avicel sample (10 g) in 20% NaOH solution for 24 h while stirring. The material developed a pale-yellow color. After 24 h, the mixture was filtered through a

sintered glass funnel. The NaOH solution filtered very slowly. A dilute HCl solution of ethanol/water (40%) was used for one rinse to bring the pH under 7. This was followed by additional washing with ethanol/water. The material was vacuum-dried at 50 °C before further use.

### Calibration set samples

Cellulose mixtures with cellulose II compositions in the range of 5 – 80% were produced using different mass fractions of Avicel PH-101 (cellulose I called Avicel I) and mercerized Avicel-PH-101 (cellulose II called Avicel II). In each case, a total mixture mass of 500 mg was produced (Table 1). This group of five samples (mixtures 1–5, Table 1) along with the Avicel I and Avicel II samples were classified as a calibration set for the cellulose II quantitation analysis. The crystallinity of the Avicel II sample was determined using XRD and the method of Nam (Nam et al. 2016) to be 78.8%. The X-ray peak at 22.0° (020) and minimum at 16° 2θ, respectively, were used for the crystalline and amorphous contributions. The first use of a Segal like equation for CrI of cellulose II, measuring the minimum at 16° 2θ, was by Ingersol (1946).

### Cellulose nanocrystal preparation

A procedure published earlier (Reiner and Rudie 2013) was used to produce CNCs. Briefly, dissolving pulp was treated with sulfuric acid (64 wt%) and heated to 45 °C for 90 min. The reaction was then quenched by transferring the suspension into a reactor containing a large amount of water. The suspension was further diluted. The CNC suspension is then neutralized by the slow addition of 5–8 wt% NaOH. The CNC solution is allowed to settle and is decanted. Upon further dilution, as the sodium sulfate concentration drops to about 1 wt%, the CNC particles begin to disperse in the solution. This aqueous suspension is then transferred to the ultrafiltration system for further purification. The CNCs are circulated through a tubular ultrafiltration system (Membrane Specialists, A19 modules), where the dilute salt/sugar solution passes through the membrane while CNCs are retained. Reverse osmosis (RO) water is added as needed to maintain the CNC concentrate at 1 wt%. Dialysis filtration is continued until the residual salt concentration is reduced to about 8 μM, (measured as 40–50 μS/cm2). This step requires about 24 h of dilution and filtration The colloidal CNC suspension is filtered using a 20 μm polypropylene, cartridge-style filter to remove dirt and concentrated to at least 5 wt% solids using the tubular ultrafiltration system. The overall yield is about 50 wt%.

### Alkali treatment of pulp

In a Berghof reactor (Berghof Inc., Eningen, Germany), air dried softwood bleached kraft pulp (SWBKP) (300 mg) was added to 40 mL of 5 or 10% NaOH solution and treated at 170 °C for 90 min. Post-treatment, the reactor was cooled by placing the vessel in a cold-water bath. The pulps were filtered through sintered glass funnels and were copiously washed with RO water until the filtered water was of neutral pH. Subsequently, the pulps were air dried at 25 °C.

**Table 1** Compositions of calibration set samples

| Sample | Mass ratio, mg Avicel I:Avicel II | Avicel II, % | Calculated crystalline cellulose II, %* | Model-based cellulose II, % | % Error** |
|---|---|---|---|---|---|
| Avicel I | 500:0 | 0 | 0 | 3.3 | NA*** |
| Mixture 1 | 475:25 | 5 | 3.94 | 5.2 | 32.0 |
| Mixture 2 | 450:50 | 10 | 7.88 | 5.6 | 28.9 |
| Mixture 3 | 400:100 | 20 | 15.8 | 14.5 | 8.2 |
| Mixture 4 | 300:200 | 40 | 31.5 | 27.7 | 12.1 |
| Mixture 5 | 100:400 | 80 | 63.0 | 62.7 | 0.5 |
| Avicel II | 0:500 | 100 | 78.8 | 78.6 | 0.3 |

*Based on XRD crystallinity of Avicel II (78.8%)

**%Error calculated from the difference between model-based cellulose II and theoretical crystalline cellulose II amounts

***NA, not applicable

Analysis by Raman spectroscopy

The calibration set and other samples were analyzed with a Bruker MultiRam FT-Raman spectrometer (Bruker Instruments Inc., Billerica, Massachusetts). This Raman system is equipped with a 1,064-nm 1,000-mW continuous wave (CW) diode-pumped Nd:YAG laser. Approximately 100 mg of each sample was pressed into a pellet with the help of a hydraulic press. To make a pellet, a compressive pressure of $276 \times 10^6$ dyn/cm$^2$ was applied. Spectra were obtained in triplicate. The laser power used for sample excitation was 600 mW, and 1,024 scans were accumulated. In all cases, Bruker OPUS 7.2 software was used to process the spectral data, these operations involved normalization, selection of a spectral region, background correction, and band integration. Background correction was performed using a 64 points OPUS "rubberband option". For plotting purposes, the spectra were converted to ASCII format and exported to Excel.

Using FT-Raman spectroscopy, a cellulose II quantitation method was developed based upon the ratios of peak intensities at 577 (cellulose II band) and 1096 cm$^{-1}$ (band due to both cellulose I and cellulose II). The ratios were plotted against the calculated % crystalline cellulose II, shown in Table 1. For calculating the peak heights, the following procedures were used. For both the bands, 577 and 1096 cm$^{-1}$, horizontal baselines were drawn from, respectively, 590 and 944 cm$^{-1}$ and the peak heights were measured. For the ratios $I_{577}/I_{1096}$, the standard deviations (SDs) were $< 2.5\%$ except for mixtures 2 and 3 where the SDs were 6 and 10%, respectively..

Analysis by X-ray

Wide-angle X-ray diffraction (XRD) profiles were recorded at the Materials Research Science and Engineering Center, University of Wisconsin, Madison using a Bruker (Billerica, MA) D8 Discover diffractometer in reflection mode with 0.5 mm beam aperture and equipped with monochromatic CuKα (λ = 1.5418 Å) point source and a VÅ NTEC-500 detector. The X-ray diffractometer beam aperture of 0.5 mm was used. In all cases, diffractograms were obtained on the same samples (in pellet form) that were previously analyzed by FT-Raman spectroscopy.

The crystallinity of the cellulose II sample (Avicel II) was determined using the XRD method of Nam (Nam et al. 2016). The X-ray peak at 22.0° and contribution at 16° 2θ representing, respectively, crystalline and amorphous contributions were used. For each of the calibration set samples (Table 1), using the Avicel II crystallinity data (78.8%, Table 1), the following Eq. was used to calculate the "calculated crystalline cellulose II" content. This value represented the actual amount of crystalline cellulose II present in the samples.

$$\%\ Calculated\ crystalline\ cellulose\ II = Crystallinity\ of\ Avicel\ II * (\%\ Avicel\ II) \quad (1)$$

where "% Avicel II" is the mass of Avicel II present in each of the samples (Table 1).

## Results and discussion

The compositions of various calibration set samples are shown in Table 1. In total, there are seven samples including two samples of the "pure" cellulose allomorphs (Avicel I and Avicel II), because the two allomorphs are not 100% crystalline, they do contain some amorphous/disordered cellulose. For Avicel I and Avicel II, the Segal crystallinities (Segal et al. 1959) were, respectively, 87.5 (Agarwal et al. 2016) and 78.8% (Table 1).

The Raman spectra, in the region 250–1550 cm$^{-1}$, of Avicel I, Avicel II, and amorphous Avicel are shown in Fig. 1 and the spectral band positions are compared in Table 2. The assignments of the bands to various internal coordinates are from literature (Wiley and Atalla 1987; Edwards et al. 1997) but it should be noted that most of the cellulose vibrational modes are highly coupled (Wiley and Atalla 1987) and therefore, the assignments are approximate. From the spectra and the Table, it can be noted that the mercerization treatment caused formation of cellulose II which leads to the appearance of several new spectral features (e.g., peaks at 353, 577, and 1463 cm$^{-1}$) and significant changes in the intensities or profiles of many Raman bands (e.g., 900 and 1263 cm$^{-1}$) all implying that molecular conformation in cellulose II is different from that of cellulose I (Atalla 1976, 1983, 1989; Schenzel and Fischer 2001; Wiley and Atalla 1987). Of the many bands characterizing this allomorph

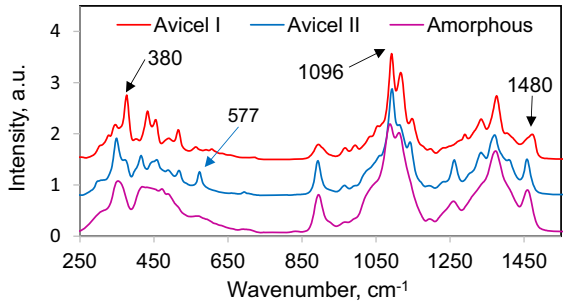


**Fig. 1** Raman spectra, in the region 250–1550 $cm^{-1}$, of Avicel I, Avicel II, and amorphous cellulose. Except for the 577 $cm^{-1}$ band, all other annotated bands are in the spectrum of Avicel I

(Table 2), the 577 $cm^{-1}$ band is unique because it does not occur in the Raman spectra of either cellulose I or amorphous cellulose (Table 2, Fig. 1). Therefore, this cellulose II Raman band was selected to develop the calibration method reported here.

Raman spectra of the two allomorphs and the five mixtures (Table 1) are shown in Figs. 2 and 3. The plotted spectra were normalized on the cellulose band at 1096 $cm^{-1}$. In Fig. 2, spectra are shown in the spectral region 250–1550 $cm^{-1}$, whereas in Fig. 3, the expanded spectra in the 577 $cm^{-1}$ region are shown so that this band can be better visualized. In the spectra of the calibration set samples, band profiles and intensities changed in the entire 250–1550 $cm^{-1}$ region. For instance, band intensities increased at 353, 577, 900, 1265, and 1462 $cm^{-1}$, these being spectral positions where cellulose II contributes in Raman spectroscopy (Agarwal 2014; Schenzel and Fisher 2001). As Avicel II content increased in the samples so did the band intensity at 577 $cm^{-1}$ (Figs. 2 and 3). The Raman intensity ratios $I_{577}/I_{1096}$ were calculated and the ratios were plotted against the % crystalline cellulose II present in the seven calibration set samples (Fig. 4). The ratios were found to be linearly correlated with the amounts of cellulose II (Fig. 2, $R^2 = 0.9944$).

Therefore, from the Raman spectrum of a sample that contains cellulose II allomorph, the following Eq. can be used to estimate the amount of crystalline cellulose II.

$$\%\ Cellulose\ II = [(I_{577}/I_{1096}) - 0.009]/0.0017 \qquad (2)$$

The model-calculated values of all the samples are shown in Table 1 and it can be noted that compared to higher cellulose II concentrations, at low concentrations the error increases (Table 1). This larger error is because not only the 577 $cm^{-1}$ peak of cellulose II becomes weaker but also because there is an increased cellulose I spectral contribution present at 577 $cm^{-1}$ from the decaying wing of the nearby cellulose I band at 567 $cm^{-1}$ (Fig. 3, Table 2). The effect of this overlap is evident in Table 1 where, in the absence of cellulose II, pure cellulose I sample still gives a value of 3.3% cellulose II. As the content of cellulose I relative to cellulose II declines, the 577 $cm^{-1}$ contribution due to the former also declines and consequently, a better match between the theoretical and the model data is obtained (Table 1).

## Comparison with XRD

To determine the usefulness of the Raman cellulose II quantitation method, it was compared with the XRD. In the latter technique, cellulose II is detected using the diffraction peaks present at 12.3, 20.5, and 22.0° 2θ (Fig. 5). Figure 5 also shows the diffraction peaks of Avicel I and from the two XRDs, it can be noted that the cellulose II and cellulose I peaks, respectively, at 22 and 22.8° 2θ overlap significantly. Moreover, the lower-2θ side decaying wing of the 22.8° cellulose I peak has some contribution in the region 20.5° 2θ where the maximum of the cellulose II peak is located (Fig. 5).

Shown in Fig. 6 are the XRDs of the calibration set samples and it can be seen that although at high Avicel II concentrations its diffraction peaks can be seen, none of the cellulose II peaks are detectable below 20 wt% concentration (Fig. 6). Compared to the 12.3° 2θ contribution, the peak at 20.5° is more easily detected although at 20 wt% composition the latter is still detected only as a weak shoulder. This is because the higher-2θ diffraction peak is more intense compared to the peak at 12.3° (Fig. 5). Nevertheless, as the concentration of Avicel II declines and the concentration of Avicel I increases, the contribution of the latter at 20.5° 2θ increases and the contribution of the former becomes unnoticeable. This observation is supported by a study that reported results of X-ray analysis of the blends of control and mercerized cotton fibers with various compositions (Nam et al. 2016). Likewise, in that study, at 20 wt% concentration of mercerized cotton fibers (cellulose II), the two diffraction peaks of the cellulose II allomorph could hardly be detected. When this detection limitation of

**Table 2** Raman frequencies (250 – 1550 $cm^{-1}$) of cellulose I, cellulose II, and amorphous cellulose

| Avicel I | Avicel II | Avicel Amorphous | Assignments* (Wiley and Atalla, 1987; Edwards et al., 1997) |
|---|---|---|---|
| –** | 308(sh) | 308(sh) | $\tau$(COH) |
| 331(sh)*** | – | – | Heavy atom bending; ring twisting |
| 348(w) | 353(m) | 356(m) | some heavy atom stretching; |
| 381(m) | 376(sh) | – | some heavy atom stretching; $\delta$(CCC) ring |
| 406 (vw) | – | – | – |
| – | 419(m) | 423(w) | – |
| 437(m) | 450(sh) | 436(sh) | some heavy atom stretching; $\nu$(CCO) ring |
| 459(m) | 461(m) | – | some heavy atom stretching; $\nu$(CCO) ring |
| – | – | 475(w) | some heavy atom stretching; $\nu$(CCO) ring |
| 492(w) | 492(w) | 492(sh) | some heavy atom stretching; $\nu$(CCO) glycosidic |
| 520(m) | 522(m) | | some heavy atom stretching; $\nu$(CCO) ring glycosidic |
| 567(w) | – | 568(sh) | some heavy atom stretching |
| – | 577(m) | – | some heavy atom stretching |
| 595(vw) | – | – | $\delta$(CCH) twisting |
| 610(vw) | – | – | $\delta$(CCH) twisting |
| 725 (vw) | – | – | – |
| 898(m) | – | – | $\nu$(COC) in plane symmetric |
| 912(sh) | – | – | HCC and HCO bending at C-6; $\nu$(COC) in plane sym |
| 971(w) | 969(w) | 970(vw) | heavy atom (CC and CO); $\rho$(CH2) |
| 997(w) | 1000(sh) | – | Stretching, C–C and C–O; $\rho$(CH2) |
| – | 1028(sh) | – | Stretching, C–C and C–O; $\nu$(CO) |
| 1037(sh) | – | – | Stretching, C–C and C–O; $\nu$(CO) primary OH |
| – | – | 1048(sh) | Stretching, C–C and C–O; $\nu$(CO) |
| 1059(sh) | 1061(sh) | – | Stretching, C–C and C–O; $\nu$(CO) secondary OH |
| 1096(s), | 1097(s) | 1092(s) | Stretching, C–C and C–O; $\nu$(COC) glycosidic asym |
| 1121(s) | 1117(sh) | 1116(s) | Stretching, C–C and C–O; $\nu$(COC) in plane sym |
| 1152(m) | 1146(m) | – | heavy atom stretching plus, HCC and HCO bending; $\nu$(CC) ring breathing asym |
| 1201(vw) | 1197(vw) | 1199(vw) | $\delta$(COH); δ(CCH) |
| 1237(vw) | 1237(vw) | – | $\delta$(COH) out of plane |
| – | 1265(m) | 1263(m) | HCC and HCO bending; $\delta$(CH2); $\delta$(CH2) twisting |
| 1294(m) | – | – | HCC and HCO bending; $\delta$(CH2) twisting |
| 1339(m) | 1338(m) | – | HCC, HCO, and HOC bending; $\delta$(CH2) |
| 1380(m) | 1374(m) | 1377(s) | HCC, HCO, and HOC bending; $\delta$(CH2) |
| 1409(sh) | 1413(sh) | – | HCC, HCO, and HOC bending; $\delta$(CH2) |
| 1463(sh) | 1462(m) | 1463(m) | HCH and HOC bending; $\delta$(CH2) scissors |
| 1476(m) | – | – | HCH and HOC bending; $\delta$(CH2) scissors |

* $\nu$ = stretching, $\delta$ = in plane scissoring, $\rho$ = in plane rocking, $\tau$ = out of plane twisting

** "——" No band present near the wavenumber position(s) of the band(s) in other columns

***Relative band intensities in a spectrum are indicated by *s* strong, *m* medium, *w* weak, *vw* very weak, *sh* shoulder

20 wt% in XRD is compared with Raman spectroscopy, the latter was found to be more sensitive because even at 5 wt% Avicel II composition, the spectral contribution at 577 $cm^{-1}$ could be detected and measured (Figs. 3 and 4).

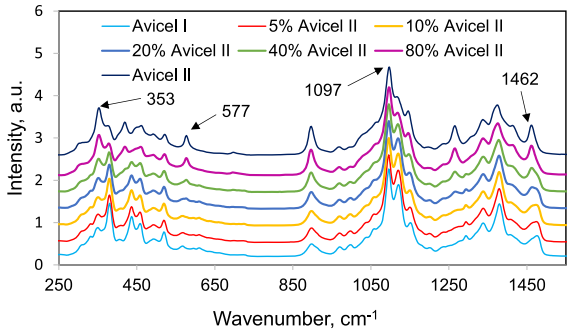


**Fig. 2** 250–1550 $cm^{-1}$ region Raman spectra of Avicel I, Avicel II, and mixtures of Avicel I and Avicel II. The annotated band positions are of Avicel II

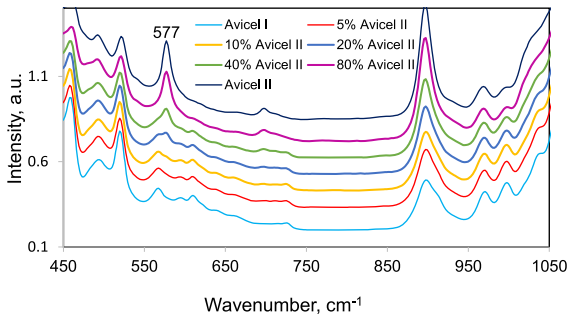


**Fig. 3** Expanded Raman spectra showing contributions at 577 $cm^{-1}$ of the seven calibration set samples

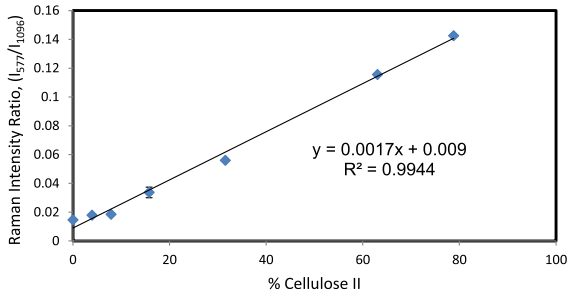


**Fig. 4** Correlation between Raman intensity ratio $I_{577}/I_{1096}$ and crystalline cellulose II content of the calibration set samples. In most cases, the SD was $< 2.5\%$

## Applications

Next, we will examine some situations where in the materials either only cellulose II is present or both cellulose I and cellulose II coexist. Additionally, amorphous cellulose is usually present in various materials unless special treatment has been carried out (e.g., acid hydrolysis). The first of the four materials discussed here (Table 2), is bleached softwood kraft

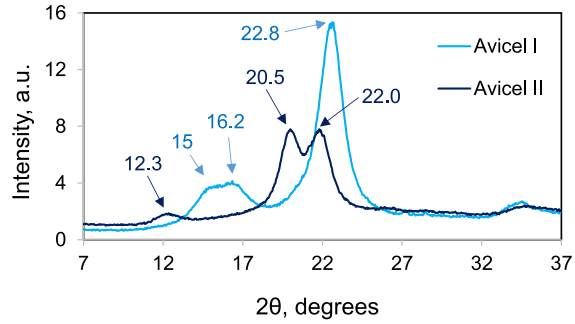


**Fig. 5** XRDs of Avicel I and Avicel II samples

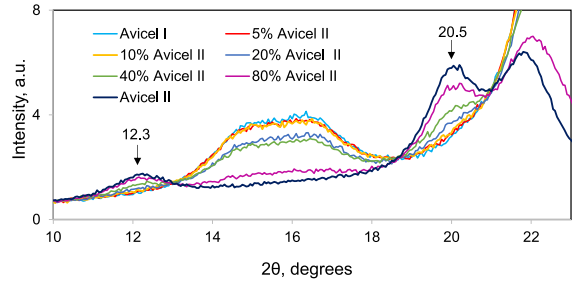


**Fig. 6** XRDs of the calibration set samples

pulp (SWBKP) which, to reduce hemicelluloses, was treated at 170 °C, at two NaOH concentrations-5% and 10%. While the lower alkali concentration did not impact the crystal lattice of the pulp fibers, treatment by the 10% alkali partially converted the pulp fibers to cellulose II type (Fig. 7). In Fig. 7, Raman spectra, in the region 250–1550 $cm^{-1}$, of control and alkali-treated pulps are shown, and it can be noted that only the pulp treated with 10% alkali showed bands at 353 and 577 $cm^{-1}$ implying that cellulose II had formed. The amount present was calculated using Eq. 2 and was found to be 35.5% as reported in Table 2. Moreover, the presence of a 380 $cm^{-1}$ peak in the spectrum of 10% NaOH treated pulp (Fig. 7) indicated that a significant amount of cellulose I survived the transformation to cellulose II.

Similarly, dissolving pulp and the CNCs produced from it using 64% $H_2SO_4$ were analyzed using Raman spectroscopy (Fig. 8). Both these materials were found to contain cellulose II (Table 2), although their concentration of cellulose II varied significantly. Compared to the CNCs, the dissolving pulp contained $\sim$ 2.5 times cellulose II (Table 3). This difference indicated that the acid hydrolysis was

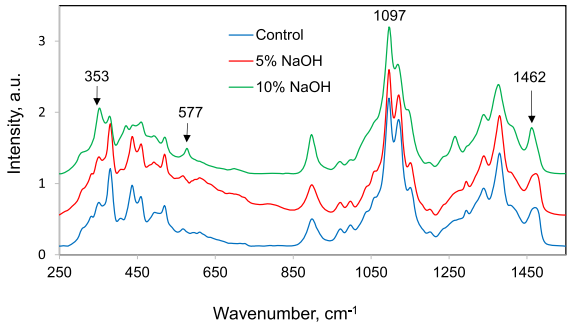


**Fig. 7** Raman spectra of untreated (control) and alkali-treated (5% and 10% NaOH) softwood bleached kraft pulps

partly successful in removing cellulose II from the substrate.

Lastly, a commercial product, Avicel C, was analyzed and was found to consist of 90% cellulose II (Table 2). Its spectrum is also shown in Fig. 8. Avicel C contained all of the spectral features of cellulose II (Table 1) including the peaks due to the H-bonded OH groups at 3445 and 3490 $cm^{-1}$ (Sturcová et al. 2003).

In summary, the calibration method developed here appears to be a reliable method for quantifying the amount of cellulose II present in the materials. The Raman method presented in this study is more sensitive than the XRD which only detects the crystallinity of cellulose II. Because, in XRD, at lower concentrations the contributions of cellulose II are quite weak (Fig. 6), it's unlikely that further processing (e.g., deconvolution) of the data would significantly improve the situation.

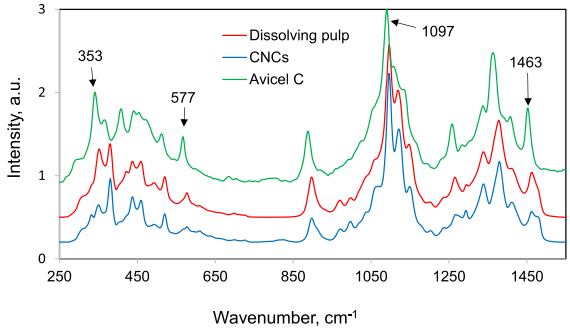


**Fig. 8** Comparison of Raman spectra of dissolving pulp and the CNCs that were derived from it. Also shown is the spectrum of Avicel C

**Table 3** Estimated amount of cellulose II

| Sample | Cellulose II, % |
|---|---|
| 10% NaOH-treated Kraft pulp | 35.5 |
| Dissolving pulp (DP) | 35.2 |
| DP CNCs | 13.6 |
| FMC Avicel C | 90.0 |

## Conclusions

FT Raman spectra and X-ray diffraction of cellulose II-containing materials were obtained. Compared to the XRD data, the 577 $cm^{-1}$ Raman peak method was found to be more sensitive for detecting cellulose II. Additionally, this band was used to develop a Raman quantitation method using a set of samples that differed in their cellulose II content. When the ratios of this peak intensity to that of the 1096 $cm^{-1}$ band $I_{577}/I_{1096}$ were correlated with the crystalline cellulose II present in the samples, an excellent correlation was obtained ($R^2 = 0.9944$). Additionally, for a number cellulose materials, this Raman correlation was used to obtain the amount of cellulose II present. It is proposed that the Raman method has the potential to estimate the amount of cellulose II allomorph in various cellulose products.

**Authors' contributions** All the authors contributed to this manuscript. UPA conceived and designed the study, carried out many of the Raman experiments, analyzed data and wrote the manuscript. SAR carried out numerous experiments and prepared cellulose II and amorphous cellulose; CB obtained the XRDs and performed data analysis; RSR prepared the cellulose nanocrystals from dissolving pulp.

**Funding** Not applicable.

**Data availability** Data and materials are available.

**Code availability** Not applicable.

**Declarations**

**Conflict of interest** There are no conflicts of interest to declare.

**Ethical approval** The article does not contain any experiments with human participants or animals performed by any of the authors.

## References


Agarwal UP (1999) An overview of Raman spectroscopy as applied to lignocellulosic materials. In: Argyropoulos DS (ed) Advances in lignocellulosics characterization. TAPPI Press, Atlanta, pp 201–225

Agarwal UP (2014) 1064 nm FT-Raman spectroscopy for investigations of plant cell walls and other biomass materials. Front Plant Sci 5:490

Agarwal UP (2019) Analysis of cellulose and lignocellulose materials by Raman spectroscopy: a review of the current status. Molecules 24:1659–1924

Agarwal UP, Ralph SA (1997) FT-Raman spectroscopy of wood: identifying contributions of lignin and carbohydrate polymers in the spectrum of black spruce (*Picea mariana*). Appl Spectro 51:1648–1655

Agarwal UP, Ralph SA, Baez C, Reiner RS (2021a) Contributions of crystalline and noncrystalline cellulose can occur in the same spectral regions: evidence based on Raman and IR and its implication for crystallinity measurements. Biomacromol 22:1357–1373

Agarwal UP, Ralph SA, Reiner RS, Baez C (2016) Probing crystallinity of never-dried wood cellulose with Raman spectroscopy. Cellulose 23:223–231

Agarwal UP, Ralph SA, Reiner RS, Baez C (2018) New cellulose crystallinity estimation method that differentiates between organized and crystalline phases. Carbohyd Polym 190:260–270

Agarwal UP, Reiner RS, Ralph SA (2010) Cellulose I crystallinity determination using FT–Raman spectroscopy: univariate and multivariate methods. Cellulose 17:721–733

Agarwal UP, Reiner RS, Ralph SA, Catchmark J, Chi K, Foster EJ, Hunt CG, Baez C, Ibach RE, Hirth KC (2021b) Characterization of the supramolecular structures of cellulose nanocrystals of different origins. Cellulose 28:1369–1385

Atalla RH (1976) Raman spectral studies of polymorphy in cellulose. Part I: celluloses I and II. Appl Poly Symp 28:659–669

Atalla RH (1983) The structure of cellulose: quantitative analysis by Raman spectroscopy. J Appl Poly Sci, Appl Poly Symp 37:295–301

Atalla RH (1989) Patterns in aggregation in native celluloses: implication of recent spectroscopic studies. In Kennedy JF, Phillips GO, Williams PA (eds) Cellulose. Ellis Horwood Chichester

Atalla RH, Gast JC, Sindorf DW, Bartuska VJ, Maciel GE (1980) Carbon-13 NMR spectra of cellulose polymorphs. J Am Chem Soc 102:3249–3251

Atalla RH, Vanderhart DL (1984) Native cellulose: A composite of two distinct crystalline forms. Science 223:283–285

Callegari A, Bolognesi S, Cecconet D, Capodaglio AG (2020) Production technologies, current role, and future prospects of biofuels feedstocks: A state-of-theart review. Crit Rev Environ Sci Technol 50:384–436

Chen C, Duan C, Li J, Liu Y, Ma X, Zheng L, Stavik J, Ni Y (2016) Cellulose (dissolving pulp) manufacturing processes and properties: a mini-review. Bio Res 11:5553–5564

Edwards HGM, Farwell DW, Webster D (1997) FT Raman microscopy of untreated natural plant fibres. Spectrochim Acta Part A 53:2383–2392

Forziati FH, Stone WK, Rowen JW, Appel WD (1950) Cotton powder for infrared transmission measurements. J Res Natl Bureau Stand 45:109–113

Foster EJ, Moon RJ, Agarwal UP, Bortner MJ, Bras J, Camarero-Espinosa S, Chan KJ, Clift MJD, Cranston ED, Eichhorn SJ, Fox DM, Hamad WY, Heux L, Jean B, Korey M, Nieh W, Ong KJ, Reid MS, Renneckar S, Roberts R, Shatkin JA, Simonsen J, Stinson-Bagby K, Wanasekara N, Youngblood J (2018) Current characterization methods for cellulose nanomaterials. Chem Soc Rev 47:2609–2679

Gierlinger N (2018) New insights into plant cell walls by vibrational microspectroscopy. Appl Spectrosc Rev 53:517–551

Haslinger S, Hietala S, Hummel M, Maunu SL, Sixta H (2019) Solid-state NMR method for the quantification of cellulose and polyester in textile blends. Carbohyd Poly 207:11–16

Hirota M, Tamura N, Saito T, Isogai A (2010) Water dispersion of cellulose II nanocrystals prepared by TEMPO-mediated oxidation of mercerized cellulose at pH 4.8. Cellulose 17:279–288

Ingersoll HG (1946) Fine structure of viscose rayon. J Appl Phys 17:924–939

Kanbayashi T, Matsunaga M, Kobayashi M (2021) Cellular-level chemical changes in Japanese beech (Fagus crenata Blume) during artificial weathering. Holzforschung. https://doi.org/10.1515/hf-2020-0229

Kesari KK, Leppänen M, Ceccherini S, Seitsonen J, Väisänen S, Altgen M, Johansson L-S, Maloney T, Ruokolainen J, Vuorinen T (2020) Chemical characterization and ultrastructure study of pulp fibers. Mater. Today Chem. 17:100224

Kumar H, Christopher LP (2010) Recent trends and developments in dissolving pulp production and application. Cellulose 24:2347–2365

Langan P, Nishiyama Y, Chanzy H (2001) X-ray Structure of Mercerized Cellulose II at 1 Å Resolution. Biomacromol 2:410–416

Morgan JJ, Craciun MF, Eichhorn SJ (2019) Quantification of stress transfer in a model cellulose nanocrystal/graphene bilayer using Raman spectroscopy. Compos Sci Technol 177:34–40

Nam S, French AD, Condon BD, Concha M (2016) Segal crystallinity index revisited by the simulation of X-ray diffraction patterns of cotton cellulose Iβ and cellulose II. Carbohyd Poly 135:1–9

Nishiyama Y, Kuga S, Okano T (2000) Mechanism of mercerization revealed by X-ray diffraction. J Wood Sci 46:452–457

Porro F, Bédué O, Chanzy H, Heux L (2007) Solid-State 13C NMR study of Na-cellulose complexes. Biomacromol 8:2586–2593

Reiner RS, Rudie AW (2013) Process scale-up of cellulose nanocrystal production to 25 kg per batch at the Forest Products Laboratory. In: Postek MT, Moon RJ, Rudie AJ, Bilodeau MA (eds) Production and applications of cellulose materials. TAPPI Press, Atlanta, pp 21–24

Schenzel K, Fischer S (2001) NIR FT Raman spectroscopy–a rapid analytical tool for detecting the transformation of cellulose polymorphs. Cellulose 8:49–57

Schenzel K, Fischer S, Brendler E (2005) New method for determining the degree of cellulose I crystallinity by means of FT Raman spectroscopy. Cellulose 12:1971–1924

Schenzel K, Almlöf H, Germgård U (2009) Quantitative analysis of the transformation process of cellulose I → cellulose II using NIR FT Raman spectroscopy and chemometric methods. Cellulose 16:407–415

Segal L, Creely JJ, Martin AE, Conrad CM (1959) An empirical method for estimating the degree of crystallinity of native cellulose using the x-ray diffractometer. Text Res J 29:786–794

Sixta H, Anne MA, Lauri HL, Shirin AS, Yibo MY, Alistair WT, King AWT, Ilkka KI, Michael HM, Ioncell F (2015) A High-strength regenerated cellulose fibre. Nord Pulp Paper Res J 30:43–57

Sturcová A, His I, Wess TJ, Cameron G, Jarvis MC (2003) Polarized vibrational spectroscopy of fiber polymers: hydrogen bonding in cellulose II. Biomacromolecules 4:1589–1595

Wada M, Heux L, Sugiyama J (2004) Polymorphism of cellulose I family: reinvestigation of cellulose $IV_I$. Biomacromol 5:1385–1391

Wada M, Nishiyama Y, Langan P (2006) X-ray structure of ammonia-cellulose I: new insights into the conversion of cellulose I to cellulose $III_I$. Macromolecules 39:2947–2952

Wiley J, Atalla RH (1987) Band assignments in the Raman spectra of celluloses. Carbohyd Res 160:113–129

Xing L, Gu J, Zhang W, Tu D, Hu C (2018) Cellulose I and II nanocrystals produced by sulfuric acid hydrolysis of Tetra pak cellulose I. Carbohyd Poly 192:184–192

Zugenmaier P (2010) Crystalline cellulose and cellulose derivatives: characterization and structures. Springer, Berlin